

# Topological Wannier Excitons in Bismuth Chalcogenide Nanosheets

F. García Flórez,<sup>1,\*</sup> Laurens D. A. Siebbeles,<sup>2,†</sup> and H. T. C. Stoof<sup>1,‡</sup>

<sup>1</sup>*Institute for Theoretical Physics and Center for Extreme Matter and Emergent Phenomena, Utrecht University, Princetonplein 5, 3584 CC Utrecht, The Netherlands*

<sup>2</sup>*Optoelectronic Materials Section, Department of Chemical Engineering, Delft University of Technology, Van der Maasweg 9, 2629 HZ Delft, The Netherlands*

(Dated: August 15, 2021)

We analyze the topology and dispersion of bulk Wannier excitons in nanosheets of topological insulators in the family of bismuth chalcogenides. Our main finding is that excitons inherit the topology of the electronic bands, quantified by the skyrmion winding numbers of the constituent electron and hole pseudospins as a function of the total exciton momentum. Every *s*-wave exciton state consists of a quartet with a degenerate and quadratically dispersing non-chiral doublet, and a chiral doublet with one linearly dispersing mode as in transition metal dichalcogenides.

*Introduction.* — Three-dimensional topological insulators, and all other topological materials for that matter, are presently receiving much attention because of their excellent prospects for energy-efficient electronics, (pseudo)spintronics devices, and quantum information processing [1–18]. Prototypical examples of three-dimensional topological insulators are the bismuth chalcogenides  $\text{Bi}_2\text{Se}_3$  and  $\text{Bi}_2\text{Te}_3$ . Since in linear response these materials are ideally conducting only due to the presence of massless Dirac fermions on their surface, most experiments with topological insulators have focussed on these unusual topologically protected surface states. Upon photoexcitation the situation, however, changes dramatically as excitons and free charges may be produced in the bulk with a topologically non-trivial band structure. Consequently it is important for light-matter interactions to investigate also the bulk properties of topological insulators and in particular the precise topological nature of the excitons whose presence or absence is crucial in optoelectronic devices, such as lasers [19–22], light-emitting diodes [23–25], and photovoltaic cells [26–29]. In the context of quantum information processing a particularly interesting question is if the exciton topology is transferred to the quantum state of the photons emitted via photo- or electro-luminescence. Apart from such applications the many-body physics of topological excitons is thought to be very exciting and accessible experimentally by well-established pump-probe techniques. Important examples of interesting many-body states are the topological excitonic insulator [30–32] and a Bose-Einstein condensate of topological excitons or possibly even biexcitons [33].

In recent years, therefore, there has been an increasing interest in the study of excitons formed in topological insulators. A pioneering approach has been to introduce, within the effective-mass approximation, Berry phase corrections to the electron-hole interaction due to the topological band structure and determine the exciton energy spectrum [34–39]. The approach presented in these works mostly focuses on the case of a total exciton momentum  $\mathbf{Q} = \mathbf{0}$ , which is sufficient for study-

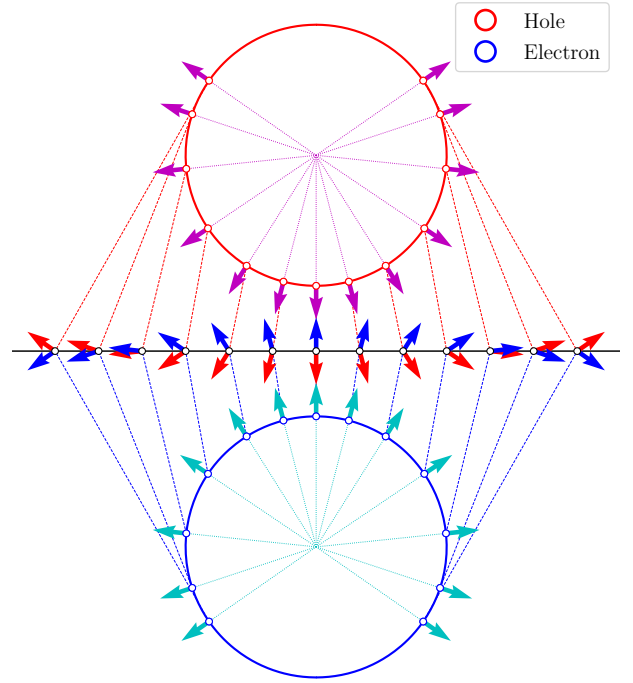


FIG. 1. Idealized illustration of the two momentum-space skyrmion textures produced by the pseudospins of the electron (bottom) and hole (top) in a weakly-bound topological exciton. Due to rotational symmetry the two circles actually represent only a radial slice of the two spheres onto which the complete momentum plane is mapped with a unit winding number. The south (north) pole of the top (bottom) sphere corresponds to the origin  $Q = 0$ , whereas the opposite pole corresponds to  $Q \rightarrow \infty$ . Note that in a normal semiconductor like CdSe the pseudospins always point in the same direction, independent of  $Q$ , and thus have no winding number.

ing optically active excitons, but not enough to obtain its global topological properties. Because of the geometry of bismuth chalcogenide nanosheets, which leads to a

lower-than-bulk dielectric constant due to the surrounding medium, we expect long-range Coulomb interactions to be enhanced thus allowing for the formation of so-called topological Wannier excitons [40, 41]. In this Letter we therefore study the concrete example of (quasi) two-dimensional bulk excitons in  $\text{Bi}_2\text{Se}_3$  nanosheets.

A main result of this work is summarized in Fig. 1, which illustrates the topologically non-trivial momentum-space pseudospin texture  $\langle \mathbf{\Gamma} \rangle_{e,h}(\mathbf{Q})$ , defined precisely below, for the electron and hole making up the exciton. This pseudospin texture gives an intuitive picture of the non-trivial topology of the exciton, as it allows us to visualize its total Chern number, as a combination of two winding numbers, by looking at the path of the electron (hole) pseudospin from pointing upwards (downwards) at the origin  $Q = 0$  to pointing downwards (upwards) at  $Q \rightarrow \infty$ , represented as the circles in Fig. 1. Thus, the pseudospin texture of each constituent particle can be seen as a skyrmion, so that the topological exciton is represented by a double skyrmion texture.

*Band structure of  $\text{Bi}_2\text{Se}_3$  nanosheets.* — Our starting point is the  $\mathbf{k} \cdot \mathbf{p}$  Hamiltonian derived in Refs. [42, 43] for modeling three-dimensional  $\text{Bi}_2\text{Se}_3$  and  $\text{Bi}_2\text{Te}_3$ . To account for the quantization in the  $z$ -direction we use a particle-in-the-box model to set the magnitude of  $k_z$  to  $\pi/L_z$ , with  $L_z$  the thickness of the nanosheet. This thickness is assumed to be sufficiently large that the Dirac states on the opposite surfaces are not gapped out by tunneling processes and the nontrivial topology of the bulk survives, but with also a sufficiently small number of quintuple layers such that electrons and holes still behave as in two-dimensions [44]. Ultimately, our Hamiltonian written in terms of Pauli matrices in spin and orbital space,  $\boldsymbol{\sigma}$  and  $\boldsymbol{\tau}$  respectively, is the  $4 \times 4$  matrix [42, 45]

$$H_0(\mathbf{k}) = \epsilon_0(\mathbf{k}) + M(\mathbf{k})\tau_z + A_2(k_x\sigma_x + k_y\sigma_y)\tau_x, \quad (1)$$

where both  $\epsilon_0(\mathbf{k}) \equiv E + D_1k_z^2 + D_2(k_x^2 + k_y^2)$  and  $M(\mathbf{k}) \equiv M - B_1k_z^2 - B_2(k_x^2 + k_y^2)$  reflect the anisotropic layered structure of the material, and the parity eigenstates  $\{|\text{Bi}^+\rangle, |\text{Se}^-\rangle\}$  span the orbital space. Note that products of matrices in different spaces, e.g.,  $\sigma_x\tau_x$ , are a tensor product instead of a matrix product and that identity matrices are implied when not specified. The values of the constants that reproduce the bulk band structure of  $\text{Bi}_2\text{Se}_3$  around the  $\Gamma$  point are  $A_2 = 0.41$  eV nm,  $M = 0.28$  eV,  $B_1 = 0.10$  eV nm<sup>2</sup>,  $B_2 = 0.57$  eV nm<sup>2</sup>,  $E = -0.0068$  eV,  $D_1 = 0.013$  eV nm<sup>2</sup>, and  $D_2 = 0.20$  eV nm<sup>2</sup>. Our results are obtained using these model parameters, except that we approximate  $B_1$  and  $D_1$  by zero as it does not affect the analysis of the topology.

Our goal is to ultimately study the topological properties of excitons, for which we need to obtain the conduction and valence bands that describe the electron and hole states. This is achieved by diagonalizing  $H_0(\mathbf{k})$ , resulting in the conduction and valence band energies

$\epsilon_{c,v}(\mathbf{k}) = \epsilon_0(\mathbf{k}) \pm \sqrt{M(\mathbf{k})^2 + A_2^2(k_x^2 + k_y^2)}$ . As a consequence of the Hamiltonian commuting with the operator  $\sigma_z\tau_z$ , the conduction and valence bands are two-fold degenerate and the eigenvalues  $\pm 1$  of  $\sigma_z\tau_z$ , denoted as the spin-orbit parity, are used to label the degenerate electronic eigenstates. Indeed,  $H_0(\mathbf{k})$  does not couple the two subspaces  $\{|\text{Bi}^+; \uparrow\rangle, |\text{Se}^-; \downarrow\rangle\}$  (even spin-orbit parity) and  $\{|\text{Bi}^+; \downarrow\rangle, |\text{Se}^-; \uparrow\rangle\}$  (odd spin-orbit parity), each subspace having a conduction and valence band at the same energies due to the spin-orbit parity invariance.

We next introduce the vector of pseudospin operators  $\mathbf{\Gamma} \equiv (\sigma_x\tau_x, \sigma_y\tau_x, \tau_z)$ , which are used to rewrite  $H_0(\mathbf{k}) = \epsilon_0(\mathbf{k}) + \mathbf{d}(\mathbf{k}) \cdot \mathbf{\Gamma}$ , with  $\mathbf{d}(\mathbf{k}) \equiv (A_2k_x, A_2k_y, M(\mathbf{k}))$ . The non-trivial topology of the Hamiltonian is now very explicit in this form, since  $\mathbf{d}(\mathbf{k})$  is a skyrmion texture in the momentum plane  $(k_x, k_y)$  and the operator  $\mathbf{\Gamma}$  reduces exactly to three Pauli matrices in the uncoupled even and odd spin-orbit-parity subspaces. The expectation value of the pseudospin as a function of  $\mathbf{k}$ , therefore, follows the non-trivial winding of  $\mathbf{d}(\mathbf{k})$  and the winding number of the latter is up to a possible sign equal to the Chern number of the conduction and valence bands.

*Exciton wavefunction.* — Ignoring the fixed wavefunction in the  $z$ -direction and redefining  $\mathbf{k} \equiv (k_x, k_y)$ , the conduction and valence states are  $\langle \mathbf{x}; i|\mathbf{k}; \alpha \rangle = (e^{i\mathbf{k}\cdot\mathbf{x}}/\sqrt{V})\langle i|\chi_{\mathbf{k}}^\alpha \rangle$ , where  $V = L_xL_y$ ,  $\alpha \in \{c, \pm; v, \pm\}$ , and the states  $|i\rangle$  denote our four-dimensional combined spin and orbital basis states. The exciton state is a bound state in the polarization [46], which in second quantization is determined by the pair correlation function

$$\begin{aligned} \langle \hat{\psi}_{c,s;i}(\mathbf{x}_1)\hat{\psi}_{v,t;j}^\dagger(\mathbf{x}_2) \rangle &= \sum_{\mathbf{k}} \Phi_{\mathbf{k}}\langle \mathbf{x}_1; i|\mathbf{k}; c, s \rangle \langle \mathbf{k}; v, t|\mathbf{x}_2; j \rangle \\ &= \frac{1}{V} \sum_{\mathbf{k}} \Phi_{\mathbf{k}} e^{i\mathbf{k}\cdot\mathbf{r}} \langle i|\chi_{\mathbf{k}}^{c,s} \rangle \langle \chi_{\mathbf{k}}^{v,t}|j \rangle, \end{aligned} \quad (2)$$

where  $s, t \in \{+, -\}$ , and  $\mathbf{r} \equiv \mathbf{x}_1 - \mathbf{x}_2$ . Here  $\Phi_{\mathbf{k}}$  is the relative wavefunction of the exciton in momentum space. For clarity we have suppressed its dependence on the spin-orbit-parity labels  $s$  and  $t$  and considered first the case of  $\mathbf{Q} = \mathbf{0}$ . In terms of electron-hole states, the conduction state is unchanged while the hole state is  $\langle j|\chi_{-\mathbf{k}}^{h,t} \rangle = \langle \chi_{\mathbf{k}}^{v,t}|j \rangle$ . In this picture the pair correlation function thus reads

$$\langle \hat{\psi}_{e,s;i}(\mathbf{x}_1)\hat{\psi}_{h,t;j}^\dagger(\mathbf{x}_2) \rangle = \frac{1}{V} \sum_{\mathbf{k}} \Phi_{\mathbf{k}} e^{i\mathbf{k}\cdot\mathbf{r}} \langle i|\chi_{\mathbf{k}}^{e,s} \rangle \langle j|\chi_{-\mathbf{k}}^{h,t} \rangle, \quad (3)$$

If desired we can then obtain also a first-quantized wavefunction, which is given by

$$\begin{aligned} \Psi_{ij}^{s,t}(\mathbf{r}) &= \frac{1}{V} \sum_{\mathbf{k}} \Phi_{\mathbf{k}} e^{i\mathbf{k}\cdot\mathbf{r}} \\ &\times \frac{1}{\sqrt{2}} \left( \langle i|\chi_{\mathbf{k}}^{e,s} \rangle_1 \langle j|\chi_{-\mathbf{k}}^{h,t} \rangle_2 - \langle i|\chi_{-\mathbf{k}}^{e,s} \rangle_2 \langle j|\chi_{\mathbf{k}}^{h,t} \rangle_1 \right). \end{aligned} \quad (4)$$

Note that interchanging particles 1 and 2, thus  $\mathbf{r} \rightarrow -\mathbf{r}$ , results in an overall minus sign, after we perform the transformation  $\mathbf{k} \rightarrow -\mathbf{k}$  and assume that the relative wavefunction is even, i.e.,  $\Phi_{\mathbf{k}} = \Phi_{-\mathbf{k}}$ . The same overall sign change appears too from the interchange of  $(e, s; i)$  with  $(h, t; j)$ , as with the correlation function in Eq. (3).

As Eqs. (2) to (4) assume total exciton momentum  $\mathbf{Q} = \mathbf{0}$ , we now generalize to  $\mathbf{Q} \neq \mathbf{0}$ . In this case the exciton wavefunction is  $\Phi_{\mathbf{Q},\mathbf{k}}$  and the electron and hole states are  $|\chi_{\mathbf{Q}/2+\mathbf{k}}^{e,s}\rangle$  and  $|\chi_{\mathbf{Q}/2-\mathbf{k}}^{h,t}\rangle$ . Together with the relative momentum states  $|\mathbf{k}\rangle_{\text{rel}}$ , they describe the exciton states  $|\mathbf{Q}; s, t\rangle$  fully in Dirac notation as

$$|\mathbf{Q}; s, t\rangle = |\mathbf{Q}\rangle \sum_{\mathbf{k}} \Phi_{\mathbf{Q},\mathbf{k}} |\mathbf{k}\rangle_{\text{rel}} |\chi_{\mathbf{Q}/2+\mathbf{k}}^{e,s}\rangle |\chi_{\mathbf{Q}/2-\mathbf{k}}^{h,t}\rangle, \quad (5)$$

where  $\langle \mathbf{R} | \mathbf{Q} \rangle = e^{i\mathbf{Q}\cdot\mathbf{R}}/\sqrt{V}$ , with  $\mathbf{R} \equiv (\mathbf{x}_1 + \mathbf{x}_2)/2$ . Each combination of the spin-orbit-parity labels  $s$  and  $t$  lead

to four distinct  $s$ -wave exciton states that represent the singlet and triplet excitons in normal semiconductors.

The topology of the exciton is now studied from the dependence of the expectation value of the pseudospin  $\langle \Gamma \rangle_e(\mathbf{Q})$  on the momentum  $\mathbf{Q}$ , obtained from Eq. (5), as

$$\langle \Gamma \rangle_e(\mathbf{Q}) = \frac{1}{V} \sum_{\mathbf{k}} |\Phi_{\mathbf{Q},\mathbf{k}}|^2 \langle \chi_{\mathbf{Q}/2+\mathbf{k}}^{e,s} | \Gamma | \chi_{\mathbf{Q}/2+\mathbf{k}}^{e,s} \rangle, \quad (6)$$

and similarly for the pseudospin of the hole.

*Exciton energy spectrum.* — Having introduced the free part of the full Hamiltonian, we proceed to analyze the electron-hole interaction potential that binds electrons and holes together to form an exciton state. The interaction potential is  $V_{s,t}^C(\mathbf{Q}; \mathbf{k}, \mathbf{k}') = V_{s,t}^D(\mathbf{Q}; \mathbf{k}, \mathbf{k}') - V_{s,t}^X(\mathbf{Q}; \mathbf{k}, \mathbf{k}')$ , where  $V^D$  and  $V^X$  denote the direct and exchange interactions, respectively. These are given by

$$V_{s,t}^D(\mathbf{Q}; \mathbf{k}, \mathbf{k}') = V^C(\mathbf{k} - \mathbf{k}') \langle \chi_{\mathbf{Q}/2+\mathbf{k}'}^{c,s} | \chi_{\mathbf{Q}/2+\mathbf{k}}^{c,s} \rangle \langle \chi_{-\mathbf{Q}/2+\mathbf{k}}^{v,t} | \chi_{-\mathbf{Q}/2+\mathbf{k}'}^{v,t} \rangle, \quad (7)$$

$$V_{s,t}^X(\mathbf{Q}; \mathbf{k}, \mathbf{k}') = V^C(\mathbf{Q}) \langle \chi_{\mathbf{Q}/2+\mathbf{k}'}^{c,s} | \chi_{-\mathbf{Q}/2+\mathbf{k}'}^{v,t} \rangle \langle \chi_{-\mathbf{Q}/2+\mathbf{k}}^{v,t} | \chi_{\mathbf{Q}/2+\mathbf{k}}^{c,s} \rangle, \quad (8)$$

where  $V^C(q) = -e^2/2\epsilon q$  is the attractive three-dimensional Coulomb potential in momentum space. We use  $\epsilon = 6$  which is typical for a low dielectric constant of the environment [47]. Note that the topology is not affected by the specific value of  $\epsilon$ . Due to the orthogonality of the states in the different spin-orbit-parity subspaces  $V^X$  only contributes when  $s = t$  and  $\mathbf{Q} \neq \mathbf{0}$ , as the inner products in Eq. (8) tend linearly to zero as a function of  $\mathbf{Q}$ . Thus, the states  $|\mathbf{Q}; +, -\rangle$  and  $|\mathbf{Q}; -, +\rangle$  are not coupled by interactions, whereas the states  $|\mathbf{Q}; +, +\rangle$  and  $|\mathbf{Q}; -, -\rangle$  are. To treat this coupling in the  $s$ -wave approximation we diagonalize the interaction matrix, giving the eigenvalues  $V_{++}^D(\mathbf{Q}; \mathbf{k}, \mathbf{k}') - V_{++}^X(\mathbf{Q}; \mathbf{k}, \mathbf{k}') \pm |V_{+-}^X(\mathbf{Q}; \mathbf{k}, \mathbf{k}')|$  which are the effective potentials for the corresponding exciton eigenstates that solve the associated Bethe-Salpeter equation [48, 49].

Ultimately, the exciton eigenstates split in this manner into two doublets as

$$\begin{aligned} |\mathbf{Q}; 0_{\pm}\rangle &\equiv \frac{1}{\sqrt{2}} (|\mathbf{Q}; +, -\rangle \pm |\mathbf{Q}; -, +\rangle), \\ |\mathbf{Q}; 2_{\pm}\rangle &\equiv \frac{1}{\sqrt{2}} (|\mathbf{Q}; +, +\rangle \pm e^{2i\phi_{\mathbf{Q}}} |\mathbf{Q}; -, -\rangle), \end{aligned} \quad (9)$$

with  $\phi_{\mathbf{Q}}$  the polar angle of  $\mathbf{Q}$  with respect to the  $x$ -axis. Our results indicate that the non-chiral doublet  $|\mathbf{0}; 0_{\pm}\rangle$  is dark, while the chiral doublet  $|\mathbf{0}; 2_{\pm}\rangle$  is bright. The reasons for this are twofold. First, for circular polarizations in the  $xy$ -plane the dipole operator is proportional to  $(\sigma_x \pm \sigma_y)\tau_x$ , which is spin-orbit parity even. It thus

couple to the states  $|\mathbf{0}; +, +\rangle$  and  $|\mathbf{0}; -, -\rangle$  and the transition matrix elements have a non-vanishing overlap with the  $s$ -wave exciton wavefunction, making the  $|\mathbf{0}; 2_{\pm}\rangle$  doublet bright [50]. Second, for linear polarization along the  $z$ -direction the dipole operator is proportional to  $\sigma_z\tau_x$ , which is spin-orbit parity odd. In principle, it couples therefore both to the states  $|\mathbf{0}; +, -\rangle$  and  $|\mathbf{0}; -, +\rangle$ , but the overlap with the transition matrix elements vanishes for  $s$ -wave excitons and consequently the  $|\mathbf{0}; 0_{\pm}\rangle$  doublet is dark. Note however that  $p$ -wave excitons are bright in this case, unlike the situation in ordinary semiconductors. Furthermore, since the interaction potentials are the same for the states in the  $|\mathbf{Q}; 0_{\pm}\rangle$  doublet, they are degenerate in energy, whereas the two states in the  $|\mathbf{Q}; 2_{\pm}\rangle$  doublet are degenerate in energy only for  $\mathbf{Q} = \mathbf{0}$ . As a result of the phase factor  $e^{2i\phi_{\mathbf{Q}}}$  in their linear superposition the states in the  $|\mathbf{Q}; 2_{\pm}\rangle$  doublet have chirality two, analogously to the situation in transition metal dichalcogenides [51–56].

Figure 2 shows the dispersion relations of all four exciton states, including several radially excited  $ns$  states. Notice the difference in behavior of the energy between the  $|\mathbf{Q}; 2_{\pm}\rangle$  and  $|\mathbf{Q}; 0_{\pm}\rangle$  doublets around  $\mathbf{Q} = \mathbf{0}$ , as the former linearly splits off which may be analytically understood by expanding the coupling term  $V_{+-}^X(\mathbf{Q}; \mathbf{k}, \mathbf{k}')$  in the effective potential around this point. The energy of the  $|\mathbf{Q}; 0_{\pm}\rangle$  doublet follows a quadratic dispersion both at small and large momenta, with a crossover taking place around the minimum of the electron-hole continuum, as

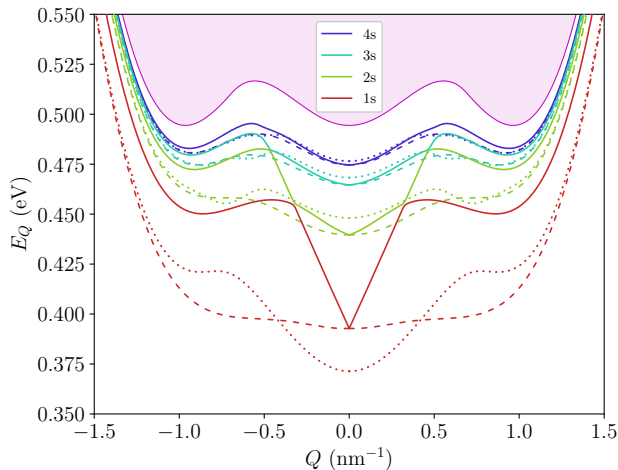


FIG. 2. Dispersion relation of the exciton states as a function of the total exciton momentum  $Q$ , for both doublets and for the first few radially excited states  $ns$ . Due to the topological band structure and its effects on the interaction potential the exciton dispersion relation shows a linear dispersion mode for the state  $|\mathbf{Q}; 2_+\rangle$ . Shown are the exciton states  $|\mathbf{Q}; 0_\pm\rangle$  (dotted line),  $|\mathbf{Q}; 2_+\rangle$  (solid line), and  $|\mathbf{Q}; 2_-\rangle$  (dashed line). The magenta region at the top represents the electron-hole continuum.

the inversion of the bands after that has less of an effect. Note that the energies of the state  $|\mathbf{Q}; 2_+\rangle$  show level repulsion in the form of avoided crossings when the energy of a given state is close to that of the next excited state. Also, the energies of the higher excited states closely follow the electron-hole continuum, as the exciton is more delocalized in real-space and their wavefunctions become those of a separate electron-hole pair.

Finally, we analyze the electron pseudospin in the various exciton states. Figure 3 shows the numerically-obtained expectation value of the pseudospin from Eq. (6), computed for each exciton state and several  $ns$  states. Comparing with Fig. 1, notice the effect of the relative exciton wavefunction on the shape of the trajectory of the pseudospin without changing the winding number. Because the pseudospins trace a (deformed) sphere the topology of the exciton is left intact, inheriting the same property from the conduction band. The pseudospin of the state  $|\mathbf{Q}; 2_+\rangle$  (solid line) contains a resonance-like feature that occurs at the avoided crossings shown in Fig. 2. However, albeit sharp-looking, both pseudospin components are still smooth continuous functions of  $Q$ .

*Conclusion and outlook.* — Our results show that the topology of the conduction and valence bands is indeed inherited by the Wannier excitons, as the exciton wavefunction contains electron and hole pseudospin textures with a topologically non-trivial winding. Furthermore, the Coulomb interaction is heavily modified by the topo-

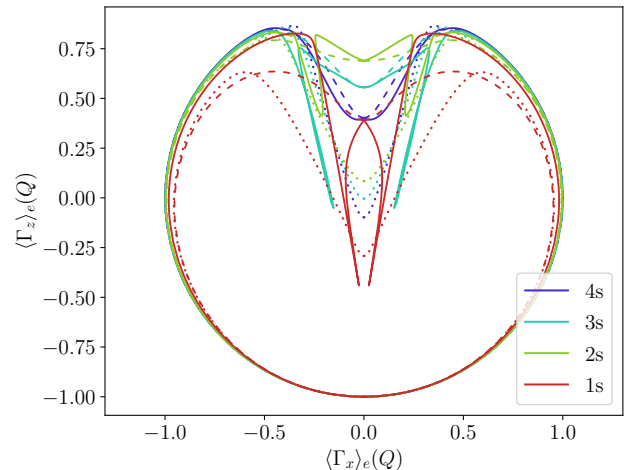


FIG. 3. Expectation of the pseudospin  $\langle \Gamma \rangle_e(\mathbf{Q})$  as a function of the total exciton momentum  $Q$  for several  $ns$  exciton states. Following the line clockwise starting from the bottom, means moving from  $Q_x \rightarrow -\infty$  towards  $Q_x \rightarrow \infty$ . Notice that due to rotational symmetry these are in fact deformed three-dimensional spheroids. Shown are the exciton states  $|\mathbf{Q}; 0_\pm\rangle$  (dotted line),  $|\mathbf{Q}; 2_+\rangle$  (solid line), and  $|\mathbf{Q}; 2_-\rangle$  (dashed line). The hole pseudospin  $\langle \Gamma \rangle_h(\mathbf{Q})$  is the  $x$ -axis mirrored image of this figure.

logical band structure and results in a non-chiral doublet with approximately quadratic dispersion relation, and a chiral doublet with one linearly dispersing state. Since our work does not impose many restrictions on the model parameters, we expect that it remains valid for other materials such as  $\text{Bi}_2\text{Te}_3$  and  $\text{Sb}_2\text{Se}_3$  by using the appropriate parameter values. A future direction of research is to consider also  $p$ -wave excitons as they are anticipated to be bright for linear polarization in the  $z$ -axis, and to consider the effects of lattice strain on the motion of the excitons, so that their Berry phase becomes visible. We also want to experimentally resolve the linear dispersion in the chiral doublet, possibly by means of terahertz and two-photon spectroscopy. Lastly, the resonance-like features around the avoided crossings that the electron pseudospin shows in Fig. 3 deserve detailed consideration.

This work is part of the research programme TOP-ECHO with project number 715.016.002, and is also supported by the D-ITP consortium. Both are programmes of the Netherlands Organisation for Scientific Research (NWO) that is funded by the Dutch Ministry of Education, Culture and Science (OCW).

\* f.garciaflores@uu.nl

† l.d.a.siebbeles@tudelft.nl

‡ h.t.c.stoof@uu.nl

- [1] L. Fu, C. L. Kane, and E. J. Mele, *Physical Review Letters* **98**, 106803 (2007).
- [2] M. Z. Hasan and C. L. Kane, *Reviews of Modern Physics* **82**, 3045 (2010).
- [3] X.-L. Qi and S.-C. Zhang, *Reviews of Modern Physics* **83**, 1057 (2011).
- [4] J. E. Moore, *Nature* **464**, 194 (2010).
- [5] B. Yan and S.-C. Zhang, *Reports on Progress in Physics* **75**, 096501 (2012).
- [6] Y. Ando, *Journal of the Physical Society of Japan* **82**, 102001 (2013).
- [7] Y. Ando and L. Fu, *Annual Review of Condensed Matter Physics* **6**, 361 (2015).
- [8] S.-Q. Shen, *Topological Insulators: Dirac Equation in Condensed Matters*, Springer Series in Solid-State Sciences (Springer-Verlag, Berlin Heidelberg, 2012).
- [9] F. Ortman, S. Roche, and S. O. Valenzuela, eds., *Topological Insulators: Fundamentals and Perspectives* (Wiley-VCH Verlag GmbH & Co. KGaA, Weinheim, 2015).
- [10] J. K. Asbóth, L. Oroszlány, and A. P. Pályi, *A Short Course on Topological Insulators: Band Structure and Edge States in One and Two Dimensions*, 1st ed., Lecture Notes in Physics No. 919 (Springer International Publishing : Imprint: Springer, Cham, 2016).
- [11] G. Tkachov, *Topological Insulators: The Physics of Spin Helicity in Quantum Transport* (Pan Stanford, Singapore, 2016).
- [12] H. Luo, ed., *Advanced Topological Insulators* (Wiley-Scrivener, Hoboken, New Jersey, 2019).
- [13] J. J. Cha, K. J. Koski, and Y. Cui, *Physica Status Solidi (RRL) – Rapid Research Letters* **7**, 15 (2013).
- [14] L.-H. Hu, R.-X. Zhang, F.-C. Zhang, and C. Wu, *Physical Review B* **102**, 235115 (2020).
- [15] L. Kou, Y. Ma, Z. Sun, T. Heine, and C. Chen, *The Journal of Physical Chemistry Letters* **8**, 1905 (2017).
- [16] C. Yue, S. Jiang, H. Zhu, L. Chen, Q. Sun, and D. W. Zhang, *Electronics* **7**, 225 (2018).
- [17] P. Liu, J. R. Williams, and J. J. Cha, *Nature Reviews Materials* **4**, 479 (2019).
- [18] M. Hohenadler and F. F. Assaad, *Journal of Physics: Condensed Matter* **25**, 143201 (2013).
- [19] Y. Ye, Z. J. Wong, X. Lu, X. Ni, H. Zhu, X. Chen, Y. Wang, and X. Zhang, *Nature Photonics* **9**, 733 (2015).
- [20] E. Y. Paik, L. Zhang, G. W. Burg, R. Gogna, E. Tutuc, and H. Deng, *Nature* **576**, 80 (2019).
- [21] C. Schneider, A. Rahimi-Iman, N. Y. Kim, J. Fischer, I. G. Savenko, M. Amthor, M. Lermer, A. Wolf, L. Worschech, V. D. Kulakovskii, I. A. Shelykh, M. Kamp, S. Reitzenstein, A. Forchel, Y. Yamamoto, and S. Höfling, *Nature* **497**, 348 (2013).
- [22] W. Wen, L. Wu, and T. Yu, *ACS Materials Letters* **2**, 1328 (2020).
- [23] S. I. Tsintzos, N. T. Pelekanos, G. Konstantinidis, Z. Hatzopoulos, and P. G. Savvidis, *Nature* **453**, 372 (2008).
- [24] D. Bajoni, E. Semenova, A. Lemaître, S. Bouchoule, E. Wertz, P. Senellart, and J. Bloch, *Physical Review B* **77**, 113303 (2008).
- [25] H. Uoyama, K. Goushi, K. Shizu, H. Nomura, and C. Adachi, *Nature* **492**, 234 (2012).
- [26] C. Adachi, M. A. Baldo, M. E. Thompson, and S. R. Forrest, *Journal of Applied Physics* **90**, 5048 (2001).
- [27] B. A. Gregg, *The Journal of Physical Chemistry B* **107**, 4688 (2003).
- [28] J. M. Luther and J. C. Johnson, *Nature* **571**, 38 (2019).
- [29] D. N. Congreve, J. Lee, N. J. Thompson, E. Hontz, S. R. Yost, P. D. Reusswig, M. E. Bahlke, S. Reineke, T. V. Voorhis, and M. A. Baldo, *Science* **340**, 334 (2013).
- [30] L. Du, X. Li, W. Lou, G. Sullivan, K. Chang, J. Kono, and R.-R. Du, *Nature Communications* **8**, 1971 (2017).
- [31] Y. Jia, P. Wang, C.-L. Chiu, Z. Song, G. Yu, B. Jäck, S. Lei, S. Klemenz, F. A. Cevallos, M. Onyszczak, N. Fishchenko, X. Liu, G. Farahi, F. Xie, Y. Xu, K. Watanabe, T. Taniguchi, B. A. Bernevig, R. J. Cava, L. M. Schoop, A. Yazdani, and S. Wu, arXiv:2010.05390 [cond-mat] (2020), arXiv:2010.05390 [cond-mat].
- [32] Z. Khatibi, R. Ahemeh, and M. Kargarian, *Physical Review B* **102**, 245121 (2020).
- [33] F. García Flórez, L. D. A. Siebbeles, and H. T. C. Stoof, *Physical Review B* **102**, 115302 (2020).
- [34] A. Hichri, S. Jaziri, and M. O. Goerbig, *Physical Review B* **100**, 115426 (2019).
- [35] M. Trushin, M. O. Goerbig, and W. Belzig, *Physical Review Letters* **120**, 187401 (2018).
- [36] J. Zhou, W.-Y. Shan, W. Yao, and D. Xiao, *Physical Review Letters* **115**, 166803 (2015).
- [37] A. Srivastava and A. Imamoglu, *Physical Review Letters* **115**, 166802 (2015).
- [38] V. A. Sablikov, *Physical Review B* **95**, 085417 (2017).
- [39] A. A. Allocca, D. K. Efimkin, and V. M. Galitski, *Physical Review B* **98**, 045430 (2018).
- [40] G. H. Wannier, *Physical Review* **52**, 191 (1937).
- [41] A. Chernikov, T. C. Berkelbach, H. M. Hill, A. Rigosi, Y. Li, O. B. Aslan, D. R. Reichman, M. S. Hybertsen, and T. F. Heinz, *Physical Review Letters* **113**, 076802 (2014).
- [42] H. Zhang, C.-X. Liu, X.-L. Qi, X. Dai, Z. Fang, and S.-C. Zhang, *Nature Physics* **5**, 438 (2009).
- [43] C.-X. Liu, H. J. Zhang, B. Yan, X.-L. Qi, T. Frauenheim, X. Dai, Z. Fang, and S.-C. Zhang, *Physical Review B* **81**, 041307(R) (2010).
- [44] F. García Flórez, L. D. A. Siebbeles, and H. T. C. Stoof, *Physical Review B* **102**, 125303 (2020).
- [45] C.-X. Liu, X.-L. Qi, H. J. Zhang, X. Dai, Z. Fang, and S.-C. Zhang, *Physical Review B* **82**, 045122 (2010).
- [46] H. Haug and S. W. Koch, *Quantum Theory of the Optical and Electronic Properties of Semiconductors* (World Scientific, Singapore ; Teaneck, N.J., 1990).
- [47] Z. Feng, Y. Hao, J. Zhang, J. Qin, L. Guo, and K. Bi, *Dielectric Properties of Two-Dimensional Bi<sub>2</sub>Se<sub>3</sub> Hexagonal Nanoplates Modified PVDF Nanocomposites*, <https://www.hindawi.com/journals/apt/2019/8720678/> (2019).
- [48] R. M. Martin, L. Reining, and D. Ceperley, *Interacting Electrons: Theory and Computational Approaches* (2016).
- [49] H. T. C. Stoof, D. B. M. Dickerscheid, and K. Gubbels, *Ultracold Quantum Fields*, Theoretical and Mathematical Physics (Springer Netherlands, 2009).
- [50] T. Cao, M. Wu, and S. G. Louie, *Physical Review Letters* **120**, 087402 (2018).
- [51] T. Yu and M. W. Wu, *Physical Review B* **89**, 205303 (2014).
- [52] H. Yu, G.-B. Liu, P. Gong, X. Xu, and W. Yao, *Nature Communications* **5**, 3876 (2014).
- [53] F. Wu, F. Qu, and A. H. MacDonald, *Physical Review B* **91**, 075310 (2015).
- [54] Z. R. Gong, W. Z. Luo, Z. F. Jiang, and H. C. Fu, Sci-

- entific Reports **7**, 42390 (2017).
- [55] D. Y. Qiu, T. Cao, and S. G. Louie, Physical Review Letters **115**, 176801 (2015).
- [56] I. Garate and M. Franz, Physical Review B **84**, 045403 (2011).